nature plants

Letter

https://doi.org/10.1038/s41477-023-01383-3

Two florigens and a florigen-like protein form a triple regulatory module at the shoot apical meristem to promote reproductive transitions in rice

Received: 4 April 2022

Accepted: 22 February 2023

Published online: 27 March 2023

Check for updates

Francesca Giaume[1,2], Giulia Ave Bono[1], Damiano Martignago[1], Yiling Miao[3], Giulio Vicentini[2], Taiyo Toriba[3], Rui Wang[4], Dali Kong[4], Martina Cerise[5], Daniele Chirivì[1], Marco Biancucci[1], Bahman Khahani[6], Piero Morandini[7], Wladimir Tameling[8], Michela Martinotti[9], Daniela Goretti[10], George Coupland[5], Martin Kater[1], Vittoria Brambilla[2], Daisuke Miki[4], Junko Kyozuka[3] & Fabio Fornara[1] ✉

Many plant species monitor and respond to changes in day length (photoperiod) for aligning reproduction with a favourable season. Day length is measured in leaves and, when appropriate, leads to the production of floral stimuli called florigens that are transmitted to the shoot apical meristem to initiate inflorescence development[1]. Rice possesses two florigens encoded by *HEADING DATE 3a* (*Hd3a*) and *RICE FLOWERING LOCUS T 1* (*RFT1*)[2]. Here we show that the arrival of Hd3a and RFT1 at the shoot apical meristem activates *FLOWERING LOCUS T-LIKE 1* (*FT-L1*), encoding a florigen-like protein that shows features partially differentiating it from typical florigens. FT-L1 potentiates the effects of Hd3a and RFT1 during the conversion of the vegetative meristem into an inflorescence meristem and organizes panicle branching by imposing increasing determinacy to distal meristems. A module comprising Hd3a, RFT1 and FT-L1 thus enables the initiation and balanced progression of panicle development towards determinacy.

Florigens, even from distantly related species, share typical features. They are transcribed and translated in phloem companion cells and are loaded into sieve elements to move as systemic long-distance signals[3,4]. Upon reaching the shoot apical meristem (SAM), they modify gene expression to start the reproductive programme. They belong to the Phosphatidyl Ethanolamine Binding Protein family[5] and regulate gene expression by forming florigen activation (or repression) complexes (FACs) upon interacting with bZIP transcription factors and Gf14 proteins[6].

In rice, flowering is accelerated upon exposure to short days (SD). Under these conditions, *HEADING DATE 1* (*Hd1*), encoding a CCT domain transcription factor, promotes the expression of the florigen-encoding genes *Hd3a* and *RICE FLOWERING LOCUS T 1* (*RFT1*) in the leaf vasculature[7]. These florigens possess all the typical features described above

[1]Department of Biosciences, University of Milan, Milan, Italy. [2]Department of Agricultural and Environmental Sciences—Production, Territory, Agroenergy, University of Milan, Milan, Italy. [3]Graduate School of Life Sciences, Tohoku University, Sendai, Japan. [4]Shanghai Center for Plant Stress Biology, Center of Excellence for Molecular Plant Sciences, Chinese Academy of Sciences, Shanghai, China. [5]Department of Plant Developmental Biology, Max Planck Institute for Plant Breeding Research, Cologne, Germany. [6]Plant Biology Graduate Program, University of Massachusetts, Amherst, MA, USA. [7]Department of Environmental Science and Policy, University of Milan, Milan, Italy. [8]Keygene N.V., Wageningen, the Netherlands. [9]Lugano Leonardo S.R.L., Tortona, Italy. [10]Umeå Plant Science Centre, Department of Plant Physiology, Umeå University, Umeå, Sweden. ✉e-mail: fabio.fornara@unimi.it

https://doi.org/10.1038/s41477-023-01383-3

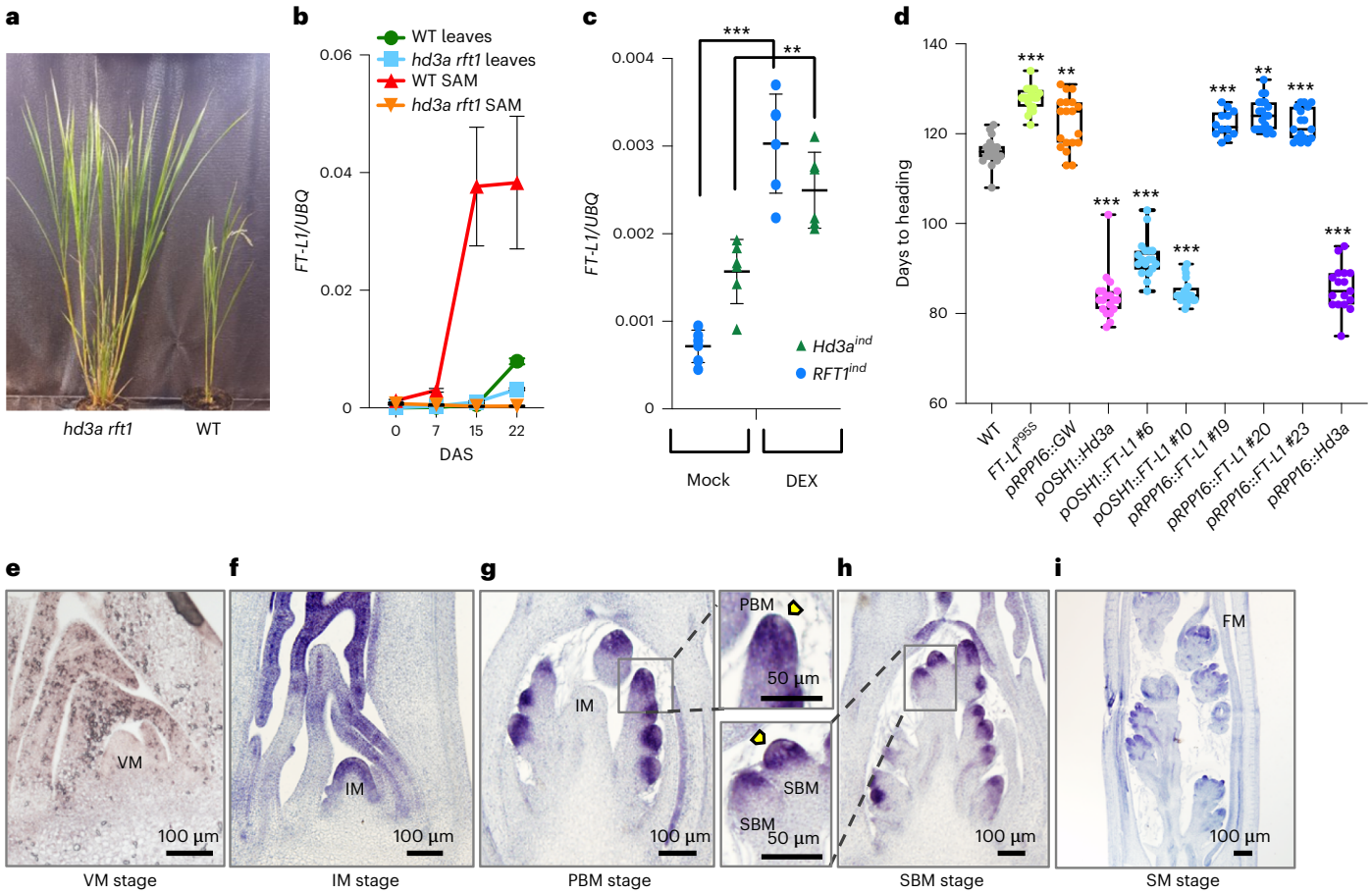

Fig. 1 | Spatio-temporal regulation of FT-L1 expression. a, A WT plant (right) and an *hd3a rft1* double mutant (left) unable to flower even after 3 years of growth under SD. **b**, Temporal expression of *FT-L1* in the SAMs and leaves of WT plants and *hd3a rft1* mutants. The samples were collected after shifting 2-month-old plants from LD to inductive SD conditions. DAS, days after shift from LD to SD. **c**, Quantification of *FT-L1* expression in meristems of *Hd3a* (*proGOS2*::*GVG 4×UAS*::*Hd3a*) and *RFT1* (*proGOS2*::*GVG 4×UAS*::*RFT1*) inducible (ind) plants, grown under LD and treated with dexamethasone (DEX) or mock. The samples were collected 16 h after the treatment. Each time point in **b** and **c** is represented as the mean ± standard deviation of two biological and three technical replicates. The values were normalized on ubiquitin (UBQ). **d**, Flowering time of Volano misexpressors of *FT-L1* and *Hd3a* under LD conditions. The background of each line is *FT-L1*^{P95S}. In each box plot, the box indicates the 25th–75th percentiles, the centre line indicates the median and the whiskers indicate the full data range. Each dot represents an independent plant measured. The statistical analysis compared misexpressors with *FT-L1*^{P95S} or *FT-L1*^{P95S} with the WT. The *P* values in **c** and **d** are based on unpaired two-tailed Student's *t*-tests with Welch correction. $^{**}P < 0.005$; $^{***}P < 0.0005$. The exact *P* values in **c** and **d** are listed in Supplementary Data 1. **e**–**i**, In situ hybridizations of *FT-L1* on WT meristems at the VM (**e**), IM (**f**), PBM (**g**) and SBM (**h**) stages. A close-up view of PBMs and SBMs is shown to highlight reduced expression at the tip (yellow arrowheads). Panel **i** shows the FM stage with floral organs already formed. The experiments were repeated twice, each time with two distinct probes that gave the same results.

and are redundant under SD[2]. Under long days (LD), flowering is mainly promoted by the expression of *RFT1* (ref. 4).

At the SAM, Hd3a and RFT1 commit the vegetative meristem (VM) to an inflorescence meristem (IM) fate, which initiates reproductive development; double *hd3a rft1* mutants never enter the flowering phase (Fig. 1a). As the IM matures, indeterminate branches develop thanks to the activity of primary branch meristems (PBMs) and secondary branch meristems (SBMs). SBMs and the apical position of PBMs form spikelet meristems (SMs), each of which develops into a determinate floret meristem (FM) forming floral organs. Meristematic fates can thus be defined by their degree of determinacy, while meristematic transitions can be regarded as progressively gaining determinacy as panicle development proceeds[8].

We identified *FLOWERING LOCUS T-LIKE 1* (*FT-L1*) among the genes whose induction is the strongest during floral commitment at the SAM[9], and this gene encodes a protein showing high amino acid sequence identity to Hd3a and RFT1 (Supplementary Fig. 1a). The overexpression of *FT-L1* under the control of a constitutive promoter induced flower development during the regeneration of plants in tissue culture, indicating strong florigenic activity, similar to that of florigens[10]. Yet, its transcription at the SAM differentiated *FT-L1* from classical florigens, whose transcription is limited to leaves, and suggested different regulation of its expression. To quantify the dynamics of *FT-L1* expression at the SAM and investigate the transcriptional dependency of *FT-L1* on florigenic signals, we measured its transcription in the SAMs of *hd3a* and *rft1* single and *hd3a rft1* double mutants during growth under SD, which promotes inflorescence development. The expression of *FT-L1* was reduced in single mutants and was more sensitive to the lack of *RFT1* (Supplementary Fig. 1d). The loss of both *Hd3a* and *RFT1* abolished *FT-L1* transcription in the SAM, indicating redundant activity of the florigens (Fig. 1b). In leaves, mild induction of *FT-L1* transcription was observed in *hd3a rft1* mutants and the wild type (WT) (Fig. 1b).

We next separated the effects of SD induction of *FT-L1* from those of Hd3a and RFT1 by quantifying *FT-L1* transcription in plants harbouring *Hd3a* (*proGOS2*::*GVG 4×UAS*::*Hd3a*, hereafter *Hd3a*^{ind})

https://doi.org/10.1038/s41477-023-01383-3

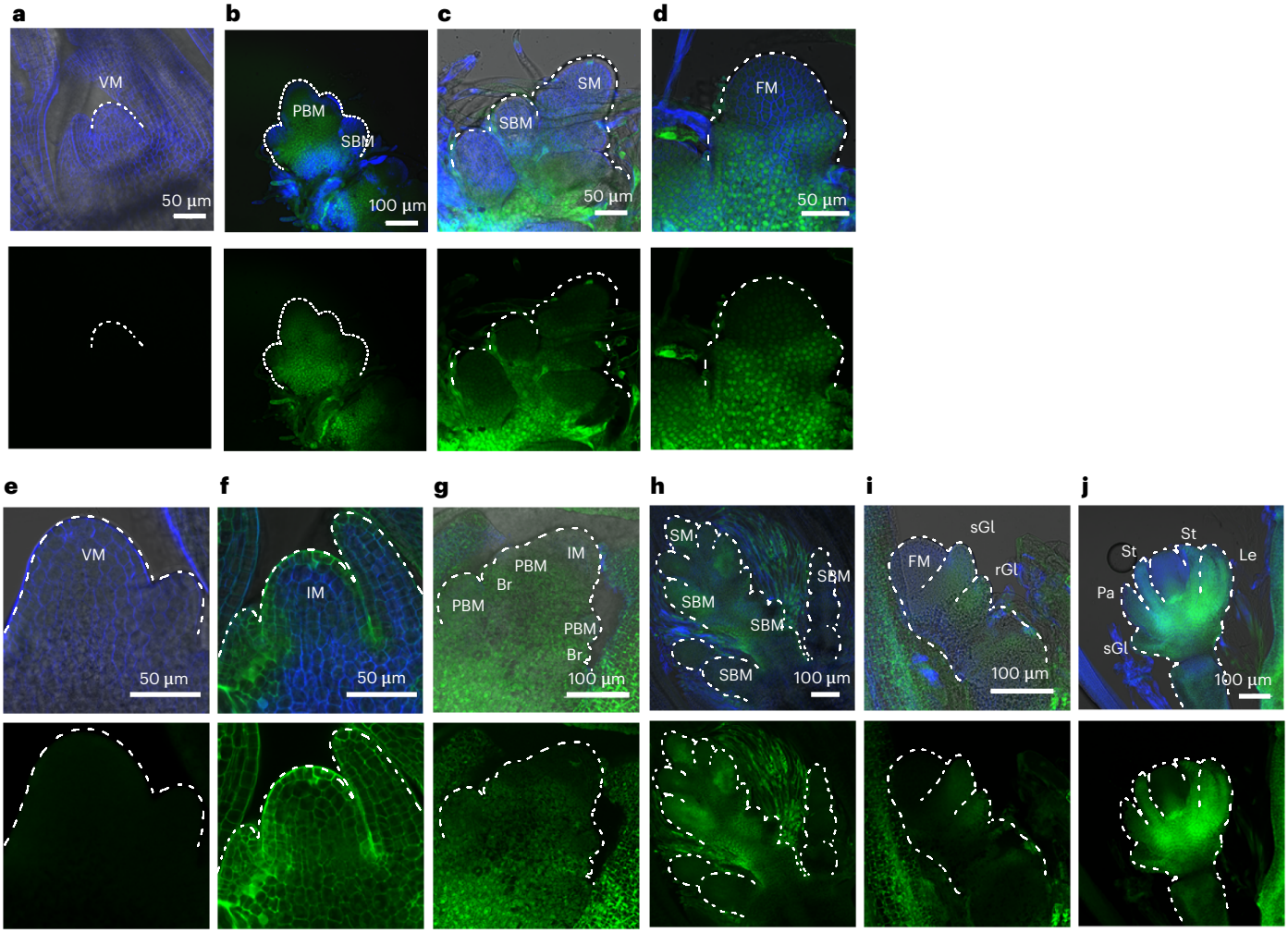

Fig. 2 | Spatial expression of FT-L1 based on reporter lines. a–**d**, Expression of *FT-L1* based on *pFT-L1*::*eYFP* transcriptional reporters shown in longitudinal sections, 50 µm thick, of shoot apices imaged at the VM (**a**), PBM and SBM (**b**), SBM and SM (**c**) and FM (**d**) stages. Three independent *pFT-L1*::*eYFP* lines gave similar results. **e**–**j**, Spatio-temporal accumulation of the FT-L1 protein based on knock-in (**e**,**f**,**h**) and *pFT-L1*::*FT-L1*::*eYFP* (**g**,**i**,**j**) reporter lines. Stages included VM (**e**), IM (**f**), PBM (**g**), SBM and SM (**h**), FM (**i**) and floral organs (**j**). St, stamen; Pa, palea; Le, lemma; rGl, rudimentary glumes; sGl, sterile glumes; Br, bract. In the confocal images, the upper pictures show all channels merged, including eYFP and GFP (green) and cell walls (Renaissance's fluorescence in blue), while the lower pictures show only the fluorescent protein channel. The experiments shown in **a**–**d** and **e**–**j** were repeated five times.

or *RFT1* (*proGOS2*::*GVG 4×UAS*::*RFT1*, hereafter $RFT1^{ind}$) inducible vectors grown under non-inductive LD[11]. The expression of *FT-L1* increased at the apex of $Hd3a^{ind}$ and $RFT1^{ind}$ plants a few hours after the leaves were treated with dexamethasone, compared with mock-treated ones (Fig. 1c). Again, induction mediated by $RFT1^{ind}$ was stronger than that induced by $Hd3a^{ind}$. Taken together, the expression data indicate that *FT-L1* is expressed at the SAM, and the florigens are necessary and sufficient for its activation. Diurnal time courses corroborated these findings, further showing high *FT-L1* transcription throughout a SD with a peak reached during the night (Supplementary Fig. 1b,c).

We next asked whether *FT-L1* induction is directly regulated by FACs containing Hd3a or RFT1. We performed chromatin immunoprecipitation (ChIP) followed by quantitative PCR with reverse transcription (RT–qPCR) on inflorescences bearing PBMs and SBMs. We used an anti-FT/TSF antibody that was previously tested to assess the specific recognition of Hd3a and RFT1 (Supplementary Fig. 2a and Supplementary Data 2). The *FT-L1* promoter contains two G-box elements, which are recognized by bZIP transcription factors. Both regions were enriched in independent ChIP experiments, indicating direct binding of the florigens (Supplementary Fig. 2b,c).

The transcription of *FT-L1* at the SAM is not consistent with a role as a systemic flowering signal moving from leaves as shown for Hd3a and RFT1. However, a specific function in the leaves could not be ruled out, because *FT-L1* expression mildly increased in leaves under SD (Fig. 1b). Similarly, it also increased in leaves under LD in early flowering genotypes bearing mutations in repressors of florigen transcription (Supplementary Fig. 1e)[12].

To understand whether leaf expression had any biological importance, we misexpressed *FT-L1* under the meristem- and stem-specific *ORYZA SATIVA HOMEOBOX 1* promoter (*pOSH1*) and under the *RICE PHLOEM PROTEIN 16* promoter (*pRPP16*), specific for companion cells and phloem parenchyma cells, in the $FT\text{-}L1^{P95S}$ mutant background (described later)[13,14]. Both *pOSH1*::*FT-L1* and *pOSH1*::*Hd3a* misexpressors flowered early compared with controls (Fig. 1d). However, *FT-L1* misexpression in the phloem could not accelerate flowering or rescue the $FT\text{-}L1^{P95S}$ mutant, while *pRPP16*::*Hd3a* plants flowered as early as meristematic misexpressors. These data suggest that *FT-L1* promotes flowering when expressed in the meristem but not in leaves. They also argue against the FT-L1 protein being a mobile systemic signal from the phloem and suggest that there is some specificity in the protein sequences of Hd3a and RFT1 that allow their movement compared with FT-L1.

We next defined the temporal and spatial accumulation of *FT-L1* transcripts and protein during panicle development. Transcripts were detected in the outer layers of the IM and in young leaf primordia, but not in the VM (Fig. 1e,f). During subsequent stages, they accumulated in PBMs and SBMs (Fig. 1g,h). Expression was not uniformly detected in these meristems; rather, it was reduced in their distal parts (magnified details in Fig. 1g,h). The signal then persisted in the flower during floral organ development (Fig. 1i). We further visualized the transcriptional pattern by expressing an eYFP under control of the *pFT-L1* promoter (*pFT-L1*::*eYFP* reporter). The expression of eYFP was detected in both primary and secondary branches and decreased in PBMs and SBMs, reaching a minimum at the tips of these meristems (Fig. 2a–c). Expression was high at the base of the spikelet and was reduced in FMs (Fig. 2d). The in situ and *pFT-L1*::*eYFP* patterns were in agreement, except for a broader eYFP expression that was evident in the centre of the main rachis and branches and did not have a corresponding signal on in situ sections.

Finally, we used two independent approaches for FT-L1 protein visualization. We generated *FT-L1*::*GFP* lines by targeted knock-in of a *GFP* sequence that replaced the stop codon[15]. In a parallel approach, we generated *pFT-L1*::*FT-L1*::*eYFP* transgenic reporters. Imaging of these lines is presented in Fig. 2e–j. FT-L1 protein accumulated in the IM, with stronger expression in the L1 layer (Fig. 2f). In subsequent stages, the protein localized in PBMs, SBMs and the bracts, with lower expression at the tips of these meristems (Fig. 2g,h). During spikelet development, FT-L1 accumulated in glume primordia but not in the FM (Fig. 2i). However, as flower development progressed, FT-L1 accumulated in floral organ primordia (Fig. 2j). Decreased expression of FT-L1 in distal cells of PBMs and SBMs suggests that it is excluded from these meristems to avoid their precocious determination and the premature specification of SM and FM that would interrupt branching. We also noted how protein localization patterns overlapped with *pFT-L1*::*eYFP* patterns. Although short-distance protein movement within reproductive meristems cannot be excluded, these data support a cell-autonomous function of FT-L1.

Overexpression and misexpression data indicate that FT-L1 can promote flowering, a typical feature of florigens. To corroborate these studies and to explore the genetic relationships between *FT-L1*, *Hd3a* and *RFT1*, we produced *ft-l1* single as well as *ft-l1 hd3a* and *ft-l1 rft1* double mutants (Supplementary Fig. 3b,c). Single *ft-l1* mutants flowered later under SD, indicating that *FT-L1* is necessary for correct timing of the VM-to-IM transition. The *ft-l1 hd3a* double mutant flowered later than *hd3a*, indicating an additive effect, whereas the *ft-l1 rft1* double mutant flowered as late as *rft1* (Fig. 3a). Under LD, *ft-l1* mutants also delayed flowering, their effect being additive to *rft1* but not to *hd3a* (Fig. 3b,c). This reversed role is consistent with the differential activities of *Hd3a* and *RFT1* depending on day length. *FT-L1* therefore acts downstream of both florigens at the VM-to-IM transition, creating a feed-forward regulatory module necessary to properly time reproductive commitment.

In mutant lines lacking FT-L1 activity, we observed alterations in panicle branching. The *ft-l1 hd3a* mutants showed a higher number of secondary branches (Fig. 3g). This phenotype and the *FT-L1* expression profile spanning all stages of panicle development suggested that *FT-L1* might also contribute to elaborate panicle architecture.

We analysed these effects using plant materials suitable for growing in field conditions, under natural photoperiods, with the additional aim of assessing potential effects on seed yield. To this end, we took advantage of NaN_3-induced mutants isolated from a Volano collection. Volano is an Italian variety adapted to high latitudes, with reduced sensitivity to the photoperiod due to mutations in *Hd1* (refs. 12,16). Using a KeyPoint 3D-based pooling technology[17], we screened 4,000 M_2 individuals by targeted amplification of *FT-L1* and amplicon sequencing (Supplementary Fig. 4a,b). We identified three missense mutants, producing the FT-L1-P95S, FT-L1-T145I and FT-L1-G117R protein variants, whose amino acid substitutions are located in highly conserved positions of the protein (Fig. 3d and Supplementary Fig. 1a)[18]. Three-dimensional structure analysis predicted that Pro95Ser and Gly117Arg modify surface charge and destabilize protein structure, whereas Thr145Ile is located in the core and does not have a predicted destabilizing effect (Supplementary Fig. 3a)[19]. The Pro95Ser substitution altered a conserved proline that in Hd3a is essential for the interaction with Gf14 proteins and is likely to have the strongest effect on protein function[6]. To investigate its functionality in FT-L1, we expressed WT and Pro95Ser mutant genes in the *ft-10* mutant of *Arabidopsis* grown in SD, under the control of the *pFD* promoter[20]. Both FT and FT-L1 misexpressors strongly accelerated flowering, while FT-L1-P95S showed weak florigenic activity (Supplementary Fig. 5).

In rice, the *FT-L1*^{P95S} and *FT-L1*^{G117R} mutants delayed flowering in both SD and natural LD conditions in field assays (Fig. 3e,f). Notably, the quantification of panicle parameters revealed that all mutations increased secondary (and some even tertiary) branch number, except for *FT-L1*^{T145I} under SD (Fig. 3h,i,l–o). Yet, *FT-L1*^{T145I} increased branching in the field, but not time to flowering, indicating that the effects of FT-L1 on flowering and branching are genetically separable and that altered panicle architecture is not just a consequence of delayed floral transition.

An increase in secondary branch number indicated that FT-L1 promotes SM identity. Its weaker activity delayed the transition from SBMs to SM, decreasing panicle determinacy and reverting SM fate to SBM fate. This interpretation is also supported by co-expression analysis that revealed high positive correlations between the expression levels of *FT-L1* and flower development genes (Supplementary Table 1).

We quantified the expression of genes marking distinct phases of inflorescence development, including Os*MADS15*, *34*, *5* and *1*, beginning to be expressed during IM commitment, final establishment of the IM, SBM formation and flower development, respectively[6,21–23]. The data indicate that the expression of Os*MADS15*, *5* and *1* was strongly reduced in *ft-l1* mutants, whereas Os*MADS34* expression was only marginally impacted (Supplementary Fig. 6).

Fig. 3 | FT-L1 promotes flowering and panicle determinacy. a, Flowering time of *ft-l1*, *hd3a ft-l1* and *rft1 ft-l1* mutants grown under SD conditions. The plants were grown for 2 months under LD conditions and then induced to flower by shifting them to SD. Days to heading were calculated starting on the day of the shift. **b**, Flowering time of *hd3a ft-l1* under LD conditions. **c**, Flowering time of *rft1 ft-l1* under LD conditions. Days to heading in **b** and **c** were measured after sowing. The graphs in **b** and **c** are separated because they refer to independent experiments. **d**, 3D structure of FT-L1, highlighting the amino acid substitutions isolated from a mutagenized collection in Volano. The modified residues are highlighted in pink. **e**,**f**, Flowering time of Volano mutants under SD (**e**) and natural LD in the field (**f**). In each box plot in **a**–**c** and **e**,**f**, the box shows the 25th–75th percentiles, the centre line indicates the median and the whiskers indicate the full data range. Each dot represents an independent plant measured. The box plots are colour-coded depending on the genotype; in **a**–**c**, the background controls are shown in gray. *P < 0.05; **P < 0.01; ***P < 0.001. The P values are based on unpaired two-tailed Student's t-tests with Welch correction. The exact P values are listed in Supplementary Data 1. **g**–**i**, Quantification of panicle branching in *hd3a ft-l1* mutants under LD (**g**) and in Volano mutants under SD (**h**) and natural LD in the field (**i**). **j**, Quantification of panicle fertility in Volano *ft-l1* mutants. Sterile flowers are those not giving rise to a caryopsis or aborting it precociously. **k**, Quantification of panicle branching in *pOSH1*::*FT-L1* and *pOSH1*::*Hd3a* misexpressor lines under LD. The data in **g**–**i** and **k** indicate the mean + standard deviation of ten panicles per genotype collected from the main culms (the means are indicated on the histograms). *P < 0.05; **P < 0.005; ***P < 0.0005. The P values are based on unpaired two-tailed Student's t-tests with Welch correction. The exact P values are listed in Supplementary Data 1. **l**–**p**, Representative panicles of the indicated genotypes. The *pOSH1*::*FT-L1* panicles (**p**) showed shattering (the shattered seeds are shown in the top right corner).

https://doi.org/10.1038/s41477-023-01383-3

We conclude that FT-L1 accelerates inflorescence development, including the VM-to-IM and SBM-to-SM transitions. Hd3a and RFT1 might not be able to guarantee sufficient determinacy to the inflorescence, thus requiring an additional downstream florigenic function. This peculiar arrangement might occur because the supply of florigens from the leaves might decrease during panicle growth

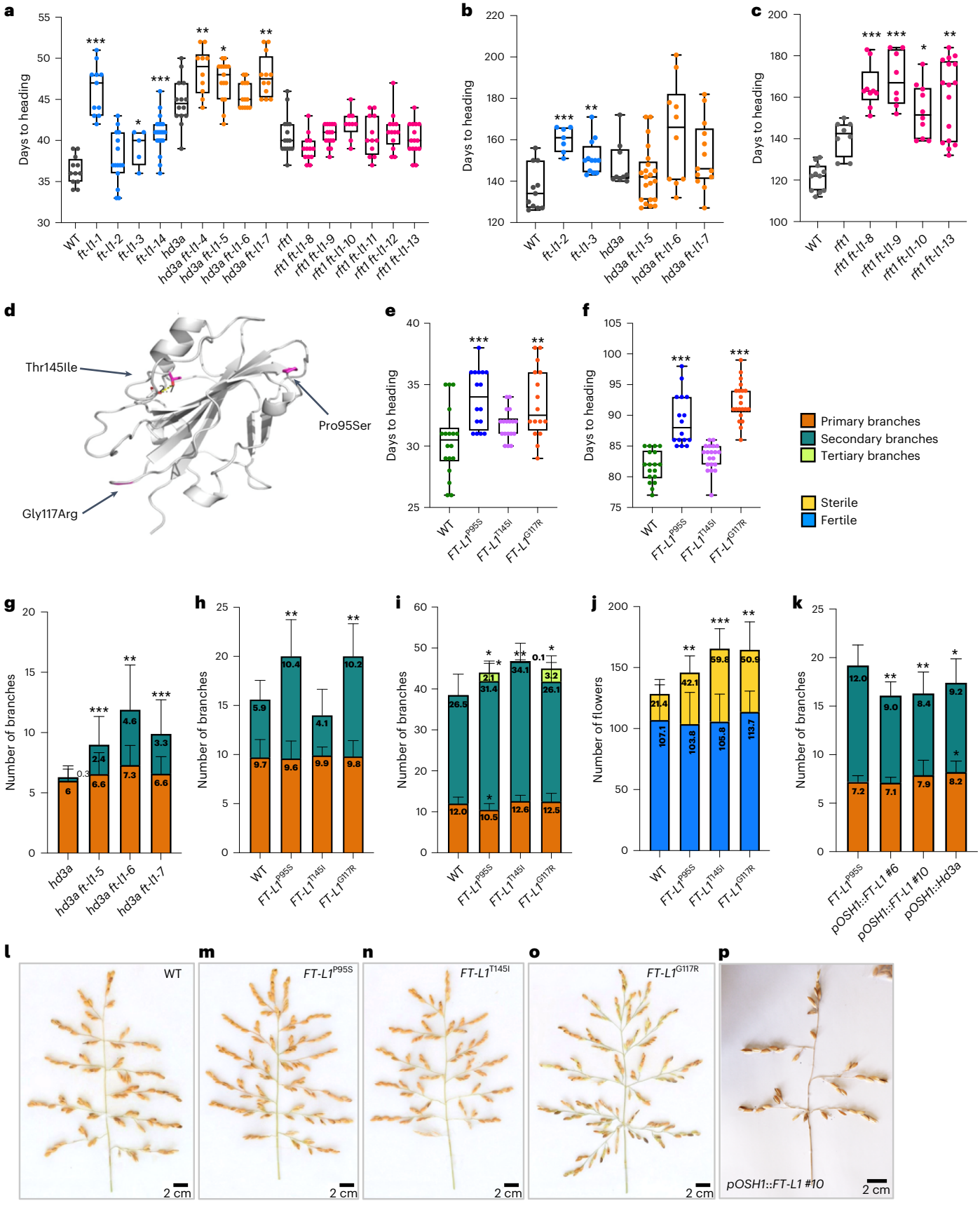

https://doi.org/10.1038/s41477-023-01383-3

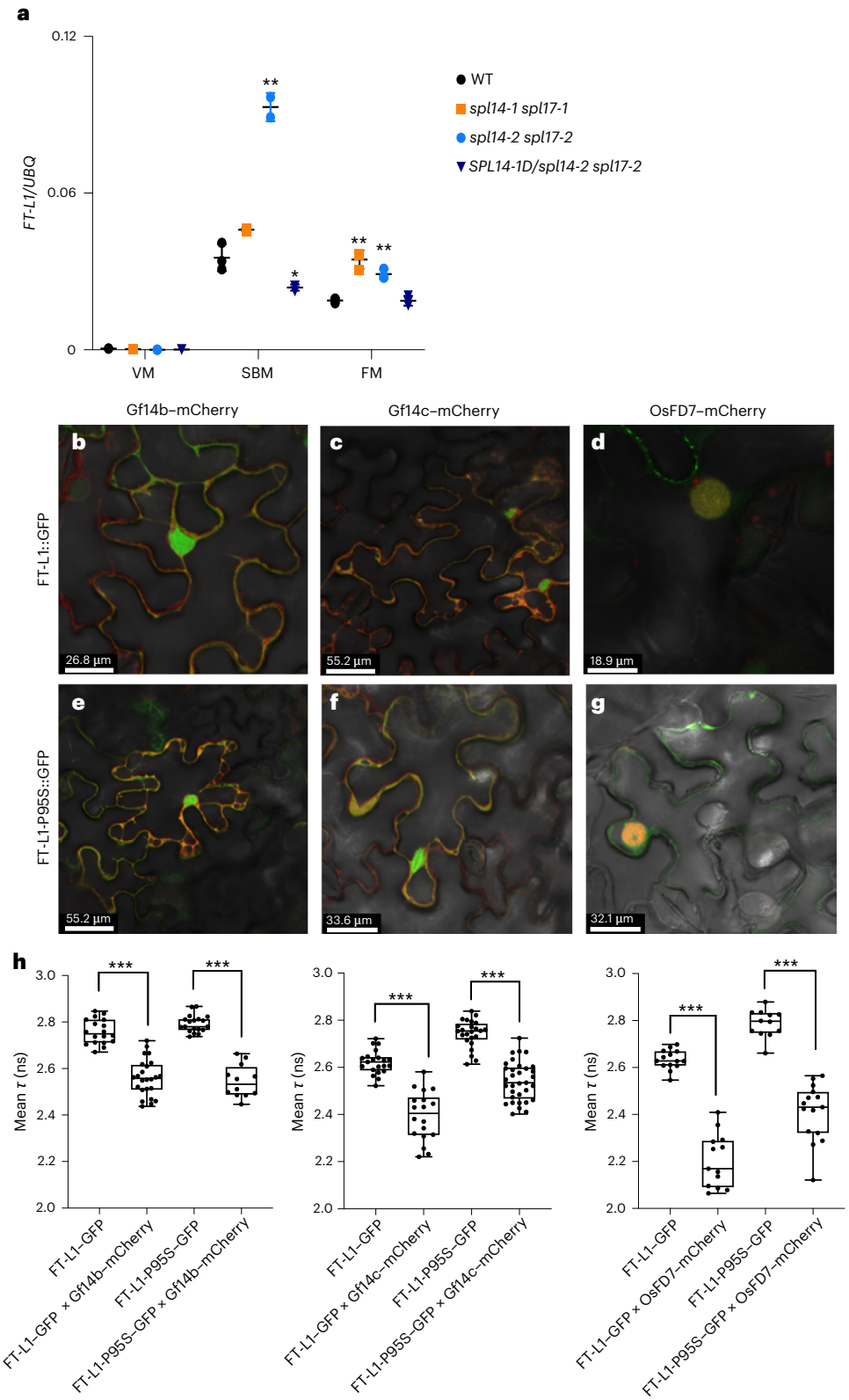

Fig. 4 | Regulation by *SPL*s and protein interactions of FT-L1. a, Quantification of *FT-L1* transcription in *SPL* loss- and gain-of-function mutant backgrounds. The data indicate the mean ± standard deviation of three technical replicates. A second biological replicate gave similar results. **b**–**g**, Co-localization patterns of FT-L1 WT (**b**–**d**) and FT-L1-P95S (**e**–**g**) with Gf14s and OsFD7. The green signal indicates FT-L1, whereas the orange signal indicates co-localization. Note that both FT-L1 forms co-localize with Gf14s only in the cytoplasm (**b**,**c**,**e**,**f**) and with OsFD7 only in the nucleus (**d**,**g**). **h**, Quantification of interaction strengths by Förster resonance energy transfer by fluorescence lifetime imaging (FRET–FLIM) measurements. Donor lifetime (τ) was quantified in nanoseconds, between FT-L1–GFP constructs without and with the Gf14s–mCherry and OsFD7–mCherry acceptors. In each box plot, the box indicates the 25th–75th percentiles, the centre line indicates the median and the whiskers indicate the full data range. Each dot indicates a measurement done on one independent cell, with at least 12 cells per combination being analysed. $^{*}P < 0.05$, $^{**}P < 0.005$, $^{***}P < 0.0005$. The *P* values are based on unpaired two-tailed Student's *t*-tests with Welch correction. All the experiments were repeated twice, with identical measurements.

and reach a level below the threshold required to terminate distal meristems at the right time.

The increase in the number of branches also determined an increase in the number of spikelets and flowers. However, a larger fraction of flowers was sterile in the mutants, consistent with FT-L1 being necessary for specifying floral identity or fertility (Fig. 3j). Grain yield therefore did not change in the mutants. To further validate these results, we performed the same analyses on the panicles of *pOSH1*::*FT-L1*. We observed a decrease in the number of secondary, but not primary, branches (Fig. 3k,p). This phenotype was shared by *pOSH1*::*Hd3a* panicles, indicating faster conversion of SBMs to SMs due to high and persistent expression of florigenic proteins during panicle development. Florigenic proteins therefore establish differential determinacy of panicle meristems, probably creating gradients along the proximo-distal axis.

The initial expression of *FT-L1* depends on Hd3a and RFT1, but its role in organizing panicle architecture at later developmental stages suggests that it might also be controlled by additional pathways. Satisfying this condition would effectively make FT-L1 a floral integrator. ChIP-seq data indicate that the *FT-L1* promoter is bound by SQUAMOSA PROMOTER BINDING PROTEIN-LIKE 14/IDEAL PLANT ARCHITECTURE 1 (SPL14/IPA1, hereafter SPL14)[24]. *SPL14* controls vegetative and reproductive branching, redundantly with *SPL17* (ref. 25). The accumulation of *SPL* transcripts is limited by *miR156/529*, and escaping such negative regulation by mutations in the *miR* target site increases panicle branching[26,27]. We asked whether SPL14 and 17 regulate *FT-L1* expression at advanced stages of panicle development. To this end, we first edited *SPL14* and *17* to produce *SPL* loss- and gain-of-function genotypes (Supplementary Fig. 7b). Next, we sampled inflorescences at the SBM and FM stages. Since mutations in *SPL*s strongly affect the timing and pattern of panicle development[28], we harvested individual samples on the basis of morphology rather than time from SD induction, and we further controlled homogeneity between and within samples by quantifying the expression level of Os*MADS15* (Supplementary Fig. 7a). *FT-L1* transcription increased in *spl14 spl17* double mutants, while it decreased when a *SPL14-D* allele was in the background, at the SBM stage (Fig. 4a). These data indicate that *SPL*s reduce *FT-L1* transcription during branching, consistent with the possibility that SPL-mediated repression of *FT-L1* is part of the mechanism that increases branch number in *SPL14* gain-of-function genotypes. Thus, *FT-L1* integrates at least the photoperiodic and SPL14 pathways to control branching.

Central to the activity of florigens is their incorporation into an FAC[6]. We carried out bimolecular fluorescence complementation (BiFC) assays to determine whether FT-L1 protein–protein interaction patterns resembled those of Hd3a and RFT1. We tested interactions with Gf14b and Gf14c, and with OsFD1, OsFD4 and OsFD7, members of the bZIP family[6,29,30]. FT-L1 interacted with Gf14s in the cytoplasm (Supplementary Fig. 8a,b) and with OsFDs in the nucleus (Supplementary Fig. 8c–e), a pattern resembling those of Hd3a and RFT1 and consistent with the observation that all amino acids forming the surface of interaction with Gf14s are conserved in Hd3a, RFT1 and FT-L1. OsFD7 interacted more strongly with FT-L1 than with Hd3a or RFT1 (refs. 11,30), and its spatio-temporal transcriptional dynamics closely matched those of *FT-L1* (Supplementary Fig. 8k–n). Most importantly, Os*FD7* RNA interference mutants had delayed flowering, increased secondary branch number and increased sterility, like *ft-l1* mutants[30]. Expression data, protein–protein interaction patterns and mutant analysis therefore suggest that the FT-L1–OsFD7 complex might determine meristem transitions in the panicle.

The FT-L1–OsFD7 dimer can assemble independently of the Gf14 bridging function[30]. In vivo interaction assays using the FT-L1-P95S mutant form indicate that FT-L1 can interact with Gf14s and OsFD7 in the same subcellular compartments (Fig. 4b–g and Supplementary Fig. 8f–h) and with the same strength as WT FT-L1 (Fig. 4h). An intact Gf14 interaction interface is therefore not necessary for FT-L1 protein contacts.

In conclusion, we have demonstrated the existence of a module comprising two florigens and one florigen-like protein that determines reproductive commitment, panicle architecture and flower fertility. The downstream element of the module shares some features with Hd3a and RFT1, including protein–protein interaction patterns, while others clearly distinguish it from classical leaf-expressed florigens, including transcription in meristems and no long-distance movement. The latter features suggest that FT-L1 has cell-autonomous activity, although this aspect needs to be further tested. In the developing panicle, FT-L1 promotes determinacy, probably in a complex with OsFD7. We propose a working model that considers a graded acquisition of meristem identities, whereby the commitment of an IM is mostly under control of FACs containing Hd3a and RFT1. Local activation of FT-L1 expression in reproductive meristems leads to the formation of FACs containing FT-L1, resulting in subsequent meristem transitions and panicle determinacy (Supplementary Fig. 9).

Methods

Plant materials and growth conditions

We used two japonica rice (*Oryza sativa*) cultivars, Nipponbare and Volano. Volano is an Italian variety insensitive to photoperiod due to a background natural mutation in the master regulator *Hd1* (refs. 12,16). Photoperiodic conditions included SD (10 h light:14 h dark) and LD (14.5 h light:9.5 h dark) for greenhouses and growth chambers (Conviron PGR15) and natural photoperiods for the paddy field. The cropping season extended from mid-April to September, and the fields were located in Tortona (44.89° N, 8.86° E). For *Arabidopsis thaliana*, the growth conditions used included only SD (10 h light:14 h dark).

In the misexpressor lines, we cloned the *FT-L1* coding sequence downstream of the 1.5 kb *pOSH1* promoter and the 1.3 kb *pRPP16* promoter in a Gateway compatible vector. The *pOSH1*::*Gateway* (*pOSH1*::*GW*) destination vector was described in ref. 11. The *pRPP16* promoter was amplified using primers pRPP16-FW and pRPP16-RV and cloned in a *pIndex4* backbone modified as described by Brambilla et al.[11]. We cloned the *FT-L1* coding sequence (531 bp) in *pDONR207* and then inserted it in the *pOSH1*::*GW* destination vector using an LRII recombination reaction. Using *pOSH1*::*FT-L1*, we excised the *pOSH1* promoter using MunI and MluI restriction enzymes. The pRPP16-FW and pRPP16-RV primers contained MunI and AscI restriction sites; we digested the fragment with MunI and AscI (an isoschizomer of MluI) and ligated the promoter into the empty vector with T4 ligase, obtaining the *pRPP16*::*FT-L1*.

The *pFT-L1*::*eYFP* vector was cloned using 2,500 bp of *pFT-L1* promoter (with primers pFT-L1 + attB1-FW and pFT-L1 + attB2-RV). The *FT-L1* promoter was inserted into *pDONR207* using BP recombinase. The *pFT-L1* entry vector was LRII-recombined into the final vector *pGWB540*, carrying the fluorophore *eYFP*. For the construction of *pFT-L1*::*FT-L1*::*eYFP*, we used a multisite gateway vector. The *FT-L1* promoter was cloned into *pDONR221* P1-P5r (with primers pFT-L1 + attB1-FW and pFT-L1 + attB5r-RV) and the *FT-L1* coding sequence (with primers OsFT-L1 + attB5-FW and OsFT-L1 + attB2-RV) into *pDONR221* P5-P2. These fragments were recombined into the final *pGWB540* using LRII recombinase. Gene targeting was performed via a sequential transformation method described in refs. 15,31,32. Briefly, the FT-L1–GFP donor construct (using primers OsFTL1-5-XbaI-FW and OsFTL1-3-EcoRI-R, sGFP-FW and sGFP-RV) was transformed into a parental rice plant line that already expressed Cas9 from a constitutive strong maize Ubiquitin 1 promoter. The FT-L1–GFP gene targeting construct harbours a homology-directed repair donor sequence with 800-bp homology arms and an OsU6-promoter-driven single guide RNA cassette targeting the FT-L1 locus. In the second transformation, T_0 transgenic calli were selected using Basta. The gene-targeting events were analysed by PCR for individual T_0 regenerated rice plants, and the

T_1 homozygous ones were used for GFP observation. The construction of the dexamethasone inducible system and treatment conditions are reported in ref. 11. The primers are listed in Supplementary Data 3.

The phenotypic analysis of panicle architecture was performed using the open-source pTRAP software (Panicle TRAit Phenotyping)[33]. The expression of *FT-L1*, *FT-L1*^{P95S} and *FT* in the *Arabidopsis ft-10* mutant was obtained using the *pFD*::*GW* vector (*pLEELA* backbone). Transgenic plants were selected with the herbicide BASTA. The resistant plants' flowering times were then recorded.

CRISPR–Cas9 editing and rice transformation

CRISPR *ft-l1* mutant lines were generated according to ref. 34 in the Nipponbare WT, as well as *hd3a-3* and *rft1-1* single mutants. *hd3a-3* and *rft1-1* are loss-of-function mutants (L. Mineri et al., manuscript in preparation). The CRISPR *ft-l1* mutants were generated by expressing a double single guide RNA, specific for *FT-L1*, considering the high homology with *Hd3a* and *RFT1*. The sequences of the single guide RNAs are highlighted in Supplementary Fig. 3c. For CRISPR-based mutagenesis of *SPL14* and *SPL17*, cloning was based on vectors described previously[35]. The selected oligonucleotide for both *SPL14* and *SPL17* is located in a region suitable for creating frame-shift mutations and *spl* loss-of-function alleles, as well as for targeting the *miR156*-binding region to obtain *SPL* gain-of-function alleles. Nipponbare and Volano calli were obtained, transformed and selected on 50 mg l^{-1} and 100 mg l^{-1} hygromycin following a published protocol[36].

RNA isolation and analysis of gene expression

We used RT–qPCR for the quantification of gene expression. SAM samples and young panicles were collected at different DAS of the plants from LD to SD conditions for inducing flowering. At least two biological replicates were processed for every time point. RNA was extracted with NucleoZOL (Macherey-Nagel) following the manufacturer's instructions. To clear the RNA samples from DNA residues, we performed a treatment with DNase I (Turbo DNase, Invitrogen). The complementary DNA was synthesized with ImProm-II Reverse Transcriptase (Promega), using 1 µg of total RNA as a starting template and a polyT primer. Quantification of the transcripts was performed with the primers listed in Supplementary Data 3, using the Maxima SYBR Green qPCR Master Mix (Thermofisher Scientific), with a RealPlex2 thermocycler (Eppendorf). The annealing temperature for all primer pairs was 60 °C. The data were analysed using MS Excel v.2211. All quantifications were calculated on the basis of technical triplicates. The *Ubiquitin* gene was used to normalize expression levels. For statistical analysis, we used *t*-tests, with a *P* value threshold of 0.05. In situ hybridizations were performed on Nipponbare WT meristems, collected at different time points. Microtome sections 7 µm thick were treated according to the protocol published by Toriba et al.[37], using 60 °C as the temperature condition for the hybridization. Two different probes were used, giving the same results (the sequences are indicated in Supplementary Data 3).

Protein–protein interaction assays

For the BiFC and FRET–FLIM assays, two- to three-week-old *Nicotiana benthamiana* plants grown at 20 °C were transfected with vectors expressing the fusion proteins of interest. The *pBAT TL-B sYFP-N* and *pBAT TL-B sYFP-C* were used for BiFC and *pABind–GFP* and *pABind–mCHERRY* for FRET–FLIM. *Agrobacterium* cultures were grown to an OD_{600} of 0.4 for BiFC and OD_{600} of 0.5 for FLIM. After agroinfiltration, the plants were incubated at 25 °C in SD conditions for two to five days. After this period, the plants were ready for BiFC imaging at the confocal. For FLIM, the plants were induced with β-estradiol with 20 µM as the final concentration, 14 to 16 hours before the confocal analysis. The GFP lifetime was measured without and with the acceptor mCherry on an average of ten transformed cells (nuclei and cytoplasm). All the experiments were repeated twice.

Confocal imaging

For the marker lines, shoot apices of the transgenic plants were collected and embedded in 6% (w/v) agarose, sliced with a Leica Vibratome VT1200S into 50-µm-thick sections and then stained with 1:1,000 Renaissance:1×PBS. A Nikon Eclipse Ti2 inverted microscope equipped with a Nikon A1R+ laser scanning device (http://www.nikon.com/) and the NIS software was used. For the imaging of knock-in marker lines, a Zeiss LSM880 laser scanning confocal microscope equipped with an Argon 488 nm laser device and the ZEN (Blue v.2.1) software was used. For the FLIM assays, a Leica MultiPhoton Falcon Dive was used with the software Leica Application Suite LAS X FLIM/FCS v.3.5.6.

Western blot and ChIP

The western blot protocol was adapted from ref. 38 as follows. Flash-frozen rice leaves were ground and homogenized in ice-cold extraction buffer (4 M urea, 50 mM Tris-HCl (pH 7.5), 150 mM NaCl, 2 mM EDTA, 0.2% β-mercaptoethanol, 0.1% SDS, cOmplete protease Inhibitor Tablet (Roche)).

Approximately 60 µg of total protein was separated on a 12% SDS–PAGE gel. For immunodetection, rabbit anti-FT (AS06 198 Agrisera) and rabbit anti-H3 (AS10 710 Agrisera) were used as the primary antibodies at 1:1,000 and 1:5,000 dilutions, respectively. Secondary anti-rabbit antibodies (AS09 602Agrisera) were used at 1:10,000 dilutions. The proteins were detected by ECL (Bio-Rad).

For ChIP–qPCR sampling, young inflorescences were collected from Nipponbare WT plants at 15 days after the shift into SD inductive conditions. Approximately 100 inflorescences were used for each replicate, and a total of two biological replicates were prepared for ChIP–qPCR. Tissue fixation, nuclei extraction and ChIP were performed as previously described by Tsuda et al.[13]. The anti-FT antibody and 2 µg of Normal Rabbit Immunoglobulin G (whole molecule, purified, FUJIFILM Wako) were used for the IP. Input samples were used as a negative control. The qPCR was performed with SYBR Green I using a Light Cycler 480 System II (Roche Applied Science).

Correlation analysis

The correlation analysis was done as described previously[39]. Briefly, the data from 728 hybridizations performed with the Affymetrix rice microarray were assembled, and the correlations among gene transcripts were measured using the Pearson correlation coefficient either on the original data or after log-transformation.

Structure and stability of FT-L1 variants

The 3D structure of WT and mutated FT-L1 was obtained by homology modelling using the tool Swiss Model (https://swissmodel.expasy.org/interactive) and monomeric AtFT (PDB ID 6igh.1) as a template. Figures of the structure were prepared with PyMOL (the PyMOL Molecular Graphics System, v.1.2r3pre, Schrödinger). To understand whether mutations in FT-L1 could impair protein stability, the homology models were analysed with DUET (http://structure.bioc.cam.ac.uk/duet).

Accession numbers

- Rice MSU Genome Annotation Project (http://rice.uga.edu)
- OsFT-L1 > LOC_Os01g11940.1
- OsHd3a > LOC_Os06g06320.1
- OsRFT1 > LOC_Os06g06300
- Gf14b> LOC_Os04g38870
- Gf14c> LOC_Os08g33370
- SPL14 > LOC_Os08g39890.1
- SPL17 > LOC_Os09g31438
- OsMADS1 > LOC_Os03g11614
- OsMADS5 > LOC_Os06g06750
- OsMADS15 > LOC_Os07g01820.1
- OsMADS34 > LOC_Os03g54170

- OsFD7 > LOC_07g48660
- OsFD4 > LOC_Os08g43600
- OsFD1 > LOC_Os09g36910
- UBQ >LOC_Os03g13170.1

Reporting summary

Further information on research design is available in the Nature Portfolio Reporting Summary linked to this article.

Data availability

All data generated or analysed during this study are included in this Letter (and its supplementary files). The 3D protein structure of FT-L1 was modelled on the basis of available structural data on monomeric AtFT (PDB ID 6igh.1).

References

1. Andrés, F. & Coupland, G. The genetic basis of flowering responses to seasonal cues. *Nat. Rev. Genet.* **13**, 627–639 (2012).
2. Komiya, R., Ikegami, A., Tamaki, S., Yokoi, S. & Shimamoto, K. Hd3a and RFT1 are essential for flowering in rice. *Development* **135**, 767–774 (2008).
3. Tamaki, S., Matsuo, S., Wong, H. L., Yokoi, S. & Shimamoto, K. Hd3a protein is a mobile flowering signal in rice. *Science* **316**, 1033–1036 (2007).
4. Komiya, R., Yokoi, S. & Shimamoto, K. A gene network for long-day flowering activates RFT1 encoding a mobile flowering signal in rice. *Development* **136**, 3443–3450 (2009).
5. Wickland, D. & Hanzawa, Y. The FLOWERING LOCUS T/TERMINAL FLOWER1 gene family: functional evolution and molecular mechanisms. *Mol. Plant* **8**, 983–997 (2015).
6. Taoka, K. et al. 14-3-3 proteins act as intracellular receptors for rice Hd3a florigen. *Nature* **476**, 332–335 (2011).
7. Yano, M. et al. Hd1, a major photoperiod sensitivity quantitative trait locus in rice, is closely related to the *Arabidopsis* flowering time gene CONSTANS. *Plant Cell* **12**, 2473–2484 (2000).
8. Whipple, C. J. Grass inflorescence architecture and evolution: the origin of novel signaling centers. *N. Phytol.* **216**, 367–372 (2017).
9. Gómez-Ariza, J. et al. A transcription factor coordinating internode elongation and photoperiodic signals in rice. *Nat. Plants* **5**, 358–362 (2019).
10. Izawa, T. et al. Phytochrome mediates the external light signal to repress FT orthologs in photoperiodic flowering of rice. *Genes Dev.* **16**, 2006–2020 (2002).
11. Brambilla, V. et al. Antagonistic transcription factor complexes modulate the floral transition in rice. *Plant Cell* **29**, 2801–2816 (2017).
12. Goretti, D. et al. Transcriptional and post-transcriptional mechanisms limit Heading Date 1 (Hd1) function to adapt rice to high latitudes. *PLoS Genet.* **13**, e1006530 (2017).
13. Tsuda, K., Ito, Y., Sato, Y. & Kurata, N. Positive autoregulation of a KNOX gene is essential for shoot apical meristem maintenance in rice. *Plant Cell* **23**, 4368–4381 (2011).
14. Asano, T. et al. Rpp16 and Rpp17, from a common origin, have different protein characteristics but both genes are predominantly expressed in rice phloem tissues. *Plant Cell Physiol.* **43**, 668–674 (2002).
15. Zhang, W. et al. Precise and heritable gene targeting in rice using a sequential transformation strategy. *Cell Rep. Methods* **3**, 100389 (2023).
16. Gómez-Ariza, J. et al. Loss of floral repressor function adapts rice to higher latitudes in Europe. *J. Exp. Bot.* **66**, 2027–2039 (2015).
17. Rigola, D. et al. High-throughput detection of induced mutations and natural variation using KeyPoint™ technology. *PLoS ONE* **4**, e4761 (2009).
18. Ho, W. W. H. & Weigel, D. Structural features determining flower-promoting activity of *Arabidopsis* FLOWERING LOCUS T. *Plant Cell* **26**, 552–564 (2014).
19. Pires, D. E. V., Ascher, D. B. & Blundell, T. L. DUET: a server for predicting effects of mutations on protein stability using an integrated computational approach. *Nucleic Acids Res.* **42**, W314-9 (2014).
20. Andrés, F. et al. SHORT VEGETATIVE PHASE reduces gibberellin biosynthesis at the *Arabidopsis* shoot apex to regulate the floral transition. *Proc. Natl Acad. Sci. USA* **111**, E2760–E2769 (2014).
21. Zhu, W. et al. Rice SEPALLATA genes OsMADS5 and OsMADS34 cooperate to limit inflorescence branching by repressing the TERMINAL FLOWER1-like gene RCN4. *N. Phytol.* **233**, 1682–1700 (2022).
22. Kobayashi, K. et al. Inflorescence meristem identity in rice is specified by overlapping functions of three AP1/FUL-like MADS box genes and PAP2, a SEPALLATA MADS box gene. *Plant Cell* **24**, 1848–1859 (2012).
23. Prasad, K., Parameswaran, S. & Vijayraghavan, U. OsMADS1, a rice MADS-box factor, controls differentiation of specific cell types in the lemma and palea and is an early-acting regulator of inner floral organs. *Plant J.* **43**, 915–928 (2005).
24. Lu, Z. et al. Genome-wide binding analysis of the transcription activator ideal plant architecture1 reveals a complex network regulating rice plant architecture. *Plant Cell* **25**, 3743–3759 (2013).
25. Wang, L. et al. Coordinated regulation of vegetative and reproductive branching in rice. *Proc. Natl Acad. Sci. USA* **112**, 15504–15509 (2015).
26. Jiao, Y. et al. Regulation of OsSPL14 by OsmiR156 defines ideal plant architecture in rice. *Nat. Genet.* **42**, 541–544 (2010).
27. Miura, K. et al. OsSPL14 promotes panicle branching and higher grain productivity in rice. *Nat. Genet.* **42**, 545–549 (2010).
28. Wang, L. et al. Bract suppression regulated by the miR156/529–SPLs–NL1–PLA1 module is required for the transition from vegetative to reproductive branching in rice. *Mol. Plant* **14**, 1168–1184 (2021).
29. Cerise, M. et al. OsFD4 promotes the rice floral transition via florigen activation complex formation in the shoot apical meristem. *N. Phytol.* **229**, 429–443 (2021).
30. Kaur, A., Nijhawan, A., Yadav, M. & Khurana, J. P. OsbZIP62/OsFD7, a functional ortholog of FLOWERING LOCUS D, regulates floral transition and panicle development in rice. *J. Exp. Bot.* **72**, 7826–7845 (2021).
31. Miki, D., Zhang, W., Zeng, W., Feng, Z. & Zhu, J. K. CRISPR/Cas9-mediated gene targeting in *Arabidopsis* using sequential transformation. *Nat. Commun.* **9**, 1967 (2018).
32. Miki, D. et al. CRISPR/Cas9-based genome editing toolbox for *Arabidopsis thaliana*. *Methods Mol. Biol.* **2200**, 121–146 (2021).
33. AL-Tam, F. et al. P-TRAP: a panicle trait phenotyping tool. *BMC Plant Biol.* **13**, 122 (2013).
34. Lowder, L. G. et al. A CRISPR/Cas9 toolbox for multiplexed plant genome editing and transcriptional regulation. *Plant Physiol.* **169**, 971–985 (2015).
35. Miao, J. et al. Targeted mutagenesis in rice using CRISPR–Cas system. *Cell Res.* **23**, 1233–1236 (2013).
36. Sahoo, K. K., Tripathi, A. K., Pareek, A., Sopory, S. K. & Singla-Pareek, S. L. An improved protocol for efficient transformation and regeneration of diverse indica rice cultivars. *Plant Methods* **7**, 49 (2011).
37. Toriba, T. et al. Suppression of leaf blade development by BLADE-ON-PETIOLE orthologs is a common strategy for underground rhizome growth. *Curr. Biol.* **30**, 509–516.e3 (2020).
38. Betti, C. et al. Sequence-specific protein aggregation generates defined protein knockdowns in plants. *Plant Physiol.* **171**, 773–787 (2016).

39. Abbruscato, P. et al. OsWRKY22, a monocot wrky gene, plays a role in the resistance response to blast. *Mol. Plant Pathol.* **13**, 828–841 (2012).

Acknowledgements

We thank G. Valè, CREA-RIS and the staff of the Botanical Garden 'Città Studi' for technical support with the field experiments and the NO LIMITS facility for technical support with confocal microscopy. We thank P. E. Colleoni for support with the molecular studies. This work was supported by the Shanghai Science and Technology Innovation Plan (grant no. 20ZR1467000) to D. Miki, by an ERC Starting Grant (no. 260963) to F.F. and by the Italy–Japan bilateral collaboration programme funded by the Italian Ministry of Foreign Affairs and International Cooperation (Grande Rilevanza, grant no. PGR10047) to F.F.

Author contributions

F.G., G.A.B., D. Martignago, Y.M., G.V., T.T., M.C., D.C., M.B., B.K., P.M., D.G. and V.B. performed the expression analyses, generated the transgenic plants, recorded the phenotypes and analysed the data. R.W., D.K. and D. Miki designed and produced the GFP knock-in plants. W.T. and M.K. produced the Volano mutant collection. M.M. performed the field experiments. G.C., V.B., D. Miki and J.K. conceived the experiments. F.F. and F.G. conceived the project and wrote the manuscript.

Competing interests

The authors declare no competing interests.

Additional information

Supplementary information The online version contains supplementary material available at https://doi.org/10.1038/s41477-023-01383-3.

Correspondence and requests for materials should be addressed to Fabio Fornara.

Peer review information *Nature Plants* thanks Richard Immink and the other, anonymous, reviewer(s) for their contribution to the peer review of this work.

nature portfolio

Corresponding author(s): Fabio Fornara

Last updated by author(s): Feb 3, 2023

Reporting Summary

Nature Portfolio wishes to improve the reproducibility of the work that we publish. This form provides structure for consistency and transparency in reporting. For further information on Nature Portfolio policies, see our Editorial Policies and the Editorial Policy Checklist.

Statistics

For all statistical analyses, confirm that the following items are present in the figure legend, table legend, main text, or Methods section.

n/a	Confirmed	
☐	☒	The exact sample size (*n*) for each experimental group/condition, given as a discrete number and unit of measurement
☐	☒	A statement on whether measurements were taken from distinct samples or whether the same sample was measured repeatedly
☐	☒	The statistical test(s) used AND whether they are one- or two-sided *Only common tests should be described solely by name; describe more complex techniques in the Methods section.*
☒	☐	A description of all covariates tested
☒	☐	A description of any assumptions or corrections, such as tests of normality and adjustment for multiple comparisons
☐	☒	A full description of the statistical parameters including central tendency (e.g. means) or other basic estimates (e.g. regression coefficient) AND variation (e.g. standard deviation) or associated estimates of uncertainty (e.g. confidence intervals)
☐	☒	For null hypothesis testing, the test statistic (e.g. *F*, *t*, *r*) with confidence intervals, effect sizes, degrees of freedom and *P* value noted *Give P values as exact values whenever suitable.*
☒	☐	For Bayesian analysis, information on the choice of priors and Markov chain Monte Carlo settings
☒	☐	For hierarchical and complex designs, identification of the appropriate level for tests and full reporting of outcomes
☐	☒	Estimates of effect sizes (e.g. Cohen's *d*, Pearson's *r*), indicating how they were calculated

Our web collection on statistics for biologists contains articles on many of the points above.

Software and code

Policy information about availability of computer code

Data collection	Gene expression data were collected using a Mastercycler RealPlex2 and software version 2.2. Confocal images were acquired using a Nikon Eclipse Ti2 inverted microscope, equipped with a Nikon A1R+ laser scanning device (http://www.nikon.com/) and the NIS software. For imaging of knock-in marker lines, a Zeiss LSM880 laser scanning confocal microscope, equipped with Argon 488nm laser device and the ZEN Blue 2.1 software was used. For FLIM assays a Leica MultiPhoton Falcon Dive was used with the software Leica Application Suite LAS X FLIM/FCS, Version 3.5.6.
Data analysis	MS Excel v.2211; GraphPad Prism v.8.0.1; P-TRAP IRD Bioinformatics (https://www.quantitative-plant.org/software/p-trap); PyMOL Molecular Graphics System, Version 1.2r3pre, Schrödinger, LLC.

For manuscripts utilizing custom algorithms or software that are central to the research but not yet described in published literature, software must be made available to editors and reviewers. We strongly encourage code deposition in a community repository (e.g. GitHub). See the Nature Portfolio guidelines for submitting code & software for further information.

Data

Policy information about availability of data

All manuscripts must include a data availability statement. This statement should provide the following information, where applicable:

- Accession codes, unique identifiers, or web links for publicly available datasets
- A description of any restrictions on data availability
- For clinical datasets or third party data, please ensure that the statement adheres to our policy

All data generated or analysed during this study are included in this published article (and its supplementary information files). Protein 3D structure of FT-L1 was modelled based on available structure of monomeric AtFT (PDB id 6igh.1).

Human research participants

Policy information about studies involving human research participants and Sex and Gender in Research.

Reporting on sex and gender	N/A
Population characteristics	N/A
Recruitment	N/A
Ethics oversight	N/A

Note that full information on the approval of the study protocol must also be provided in the manuscript.

Field-specific reporting

Please select the one below that is the best fit for your research. If you are not sure, read the appropriate sections before making your selection.

☒ Life sciences ☐ Behavioural & social sciences ☐ Ecological, evolutionary & environmental sciences

For a reference copy of the document with all sections, see nature.com/documents/nr-reporting-summary-flat.pdf

Life sciences study design

All studies must disclose on these points even when the disclosure is negative.

Sample size	flowering time data were collected from 10 plants/genotype, at least. Gene expression was quantified using three technical replicates.
Data exclusions	No data were excluded, no pre-exclusion criteria were determined.
Replication	Experimental findings were reproduced by, at least, one biological repetition of the experiment. Results of biological replicates were consistent among them.
Randomization	Plants were allocated randomly among groups.
Blinding	No blinding was performed. Several different researchers collected the data under various conditions and repeated the experiments. We exclude biases in data collection.

Reporting for specific materials, systems and methods

We require information from authors about some types of materials, experimental systems and methods used in many studies. Here, indicate whether each material, system or method listed is relevant to your study. If you are not sure if a list item applies to your research, read the appropriate section before selecting a response.

Materials & experimental systems

n/a	Involved in the study
☐	☒ Antibodies
☒	☐ Eukaryotic cell lines
☒	☐ Palaeontology and archaeology
☒	☐ Animals and other organisms
☒	☐ Clinical data
☒	☐ Dual use research of concern

Methods

n/a	Involved in the study
☒	☐ ChIP-seq
☒	☐ Flow cytometry
☒	☐ MRI-based neuroimaging

Antibodies

Antibodies used

For immunodetection, rabbit anti-FT (AS06 198 Agrisera), rabbit anti-H3 (AS10 710 Agrisera) were used as primary antibodies at 1:1,000 and 1:5,000 dilutions, respectively. Secondary anti-rabbit antibodies (AS09 602Agrisera) were used at 1:10,000 dilutions. For chromatin immunoprecipitation Normal Rabbit Immunoglobulin G (IgG) (whole molecule, purified, FUJIFILM Wako Code No.14-0955) was used.

Validation

Primary antibody was first tested on rice lines overproducing the protein of interest and on mutants that do not produce the protein.